Effect of carbon nanofillers on the mechanical and functional properties of bioderived poly(alkylene furanoate)-based films

UNIVERSITÀ DI TRENTO
Department of Industrial Engineering

Giulia Fredi, Andrea Dorigato, Mauro Bortolotti, Dimitrios N. Bikiaris, Riccardo Checchetto, Alessandro Pegoretti

Poly(alkylene 2,5-furandicarboxylate)s

- the most promising **bioderived alternative** to fossil-based poly(alkylene terephthalates) (PATs)
- superior thermo-mechanical and **gas barrier** properties than those of the corresponding PATs
- strong industrial interest: the "sleeping giant" in the world of bioplastics

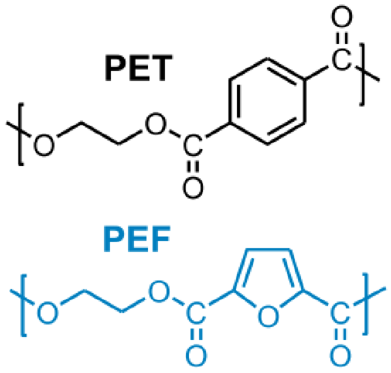

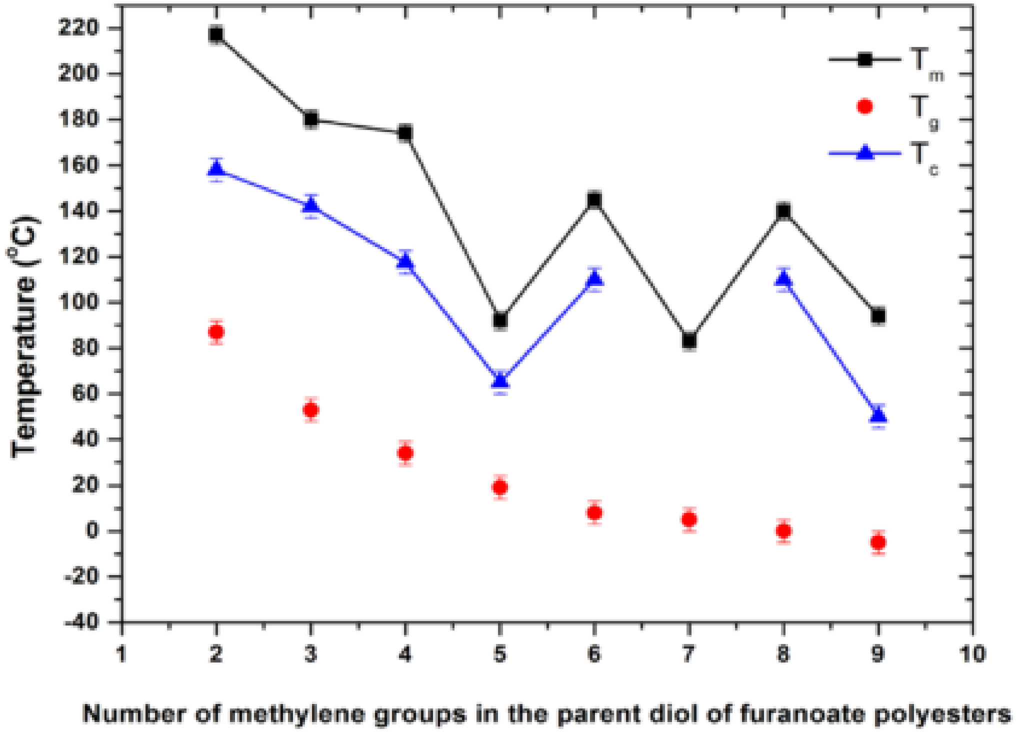

V. Tsanaktsis et al., *Materials Letters*, **2016**, 178, 64-67.

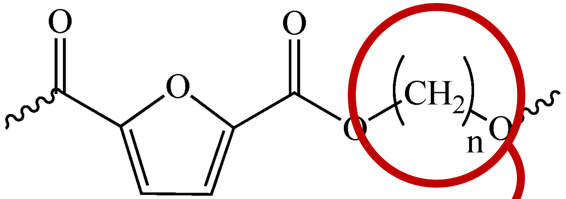

diol alkyl chain: n = 2 - 12

longer diol alkyl chain
higher molecular mobility

- lower T_g and T_m
- faster crystallization
- higher ductility

PAFs @UniTrento DII

- PAFs @UniTrento DII
  - Bulk/films for rigid and flexible packaging
    - Solution casting
      - PDeF + CNTs
      - PLA/PDoF/rGO
      - PLA/PDeF/rGO
      - PLA/PAFs
    - Melt processing
      - compatibilized PLA/PEF
      - compatibilized PLA/PPeF
  - Fibers for textile applications
    - Solution spinning
      - PLA/PAFs
    - Melt spinning
      - compatibilized PLA/PPF
      - compatibilized PLA/PBF
  - Nanofibers for biomedical applications
    - Electrospinning
      - PBF
      - PPeF

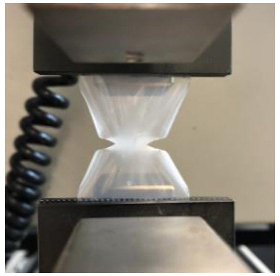

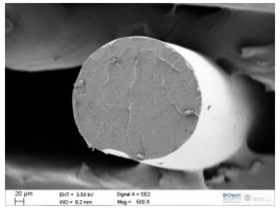

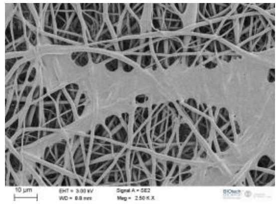

PAFs @UniTrento DII

Today’s presentation:

PDeF + CNTs

PLA/PDoF/rGO

PLA/PDeF/rGO

PLA/PAFs

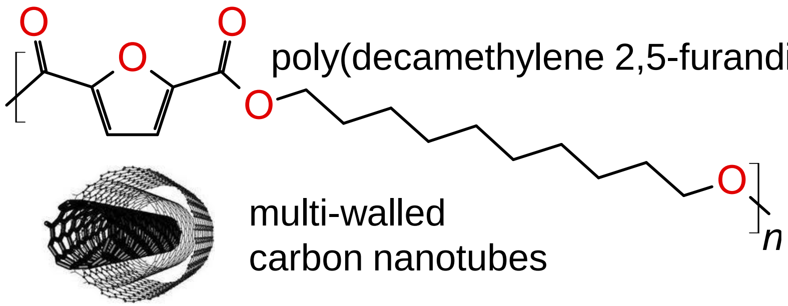

poly(decamethylene 2,5-furandicarboxylate)

multi-walled
carbon nanotubes

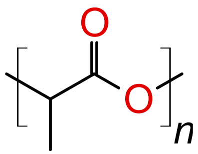

polylactide

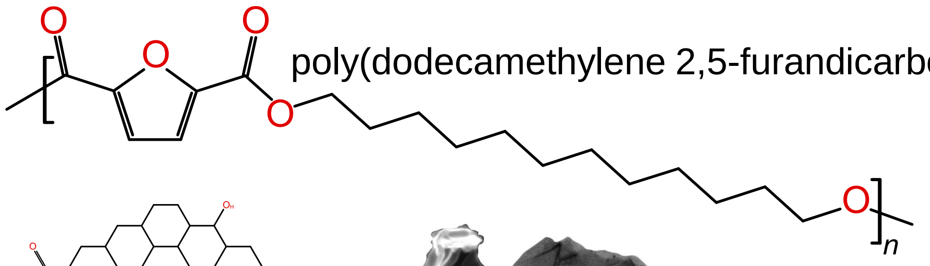

poly(dodecamethylene 2,5-furandicarboxylate)

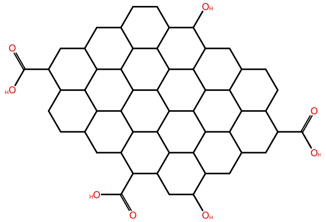

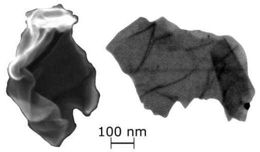

reduced graphene oxide

1. PDeF + CNTs

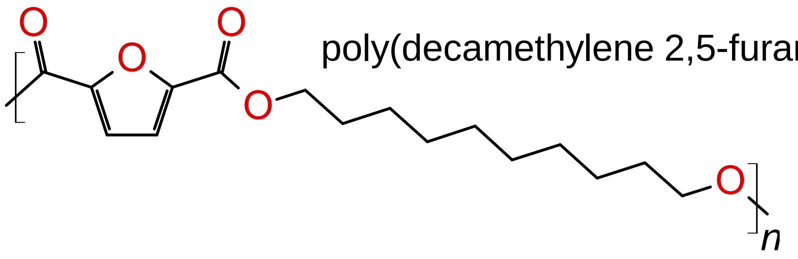

poly(decamethylene 2,5-furandicarboxylate)

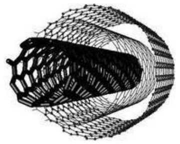

multi-walled carbon nanotubes

Poly(decamethylene furanoate)/CNTs

→ **PDeF + MWCNT** (0 – 2 phr)

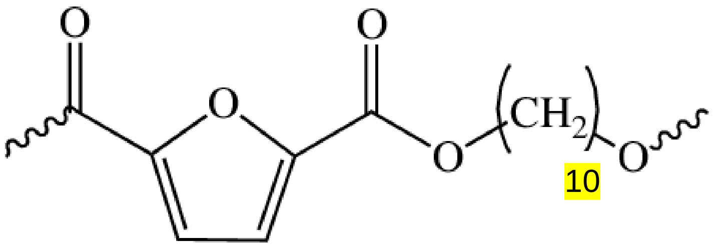

T_g = 0 °C
T_m = 110 °C

→ **Processing**: solution blending + solution casting

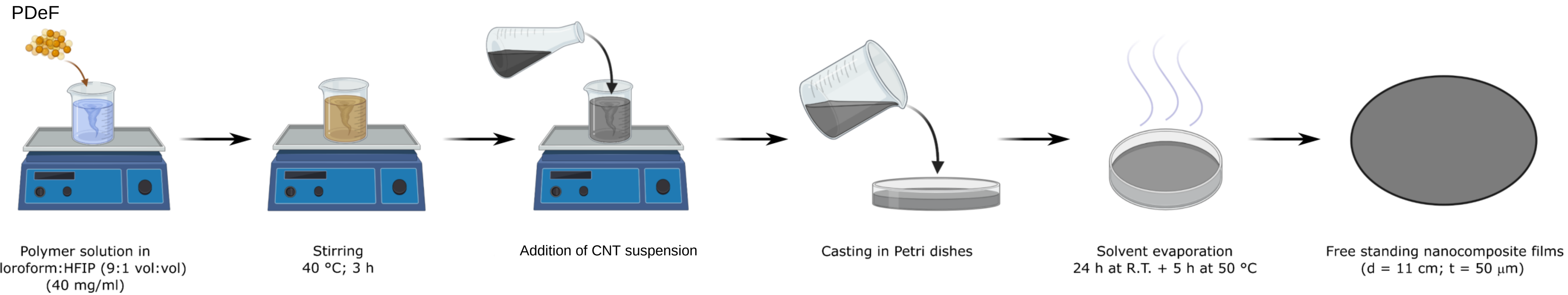

G. Fredi et al., Polymers ***2020****, 12(11), 2459*

Microstructure

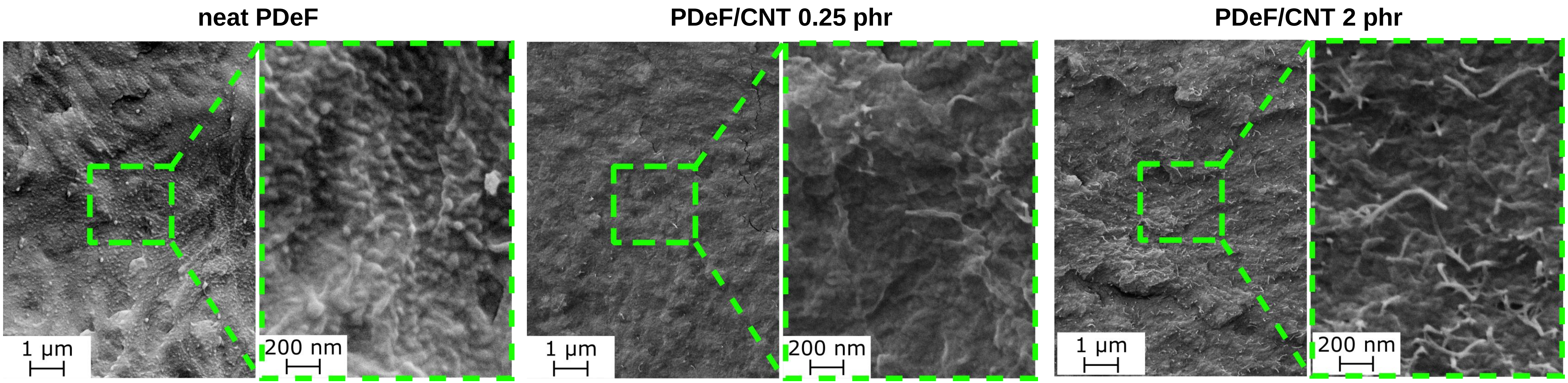

FE-SEM Zeiss Supra 60; cryofracture surfaces

- smoother and more homogeneous fracture surface
- single CNTs: good disentanglement and dispersion

G. Fredi et al., Polymers ***2020****, 12(11), 2459*

X-Ray diffraction (XRD)

Italstructures IPD3000; Cobalt anode X-Ray source ($Co_{k\alpha}$ = 1.788965 Å); 40 kV, 20 mA

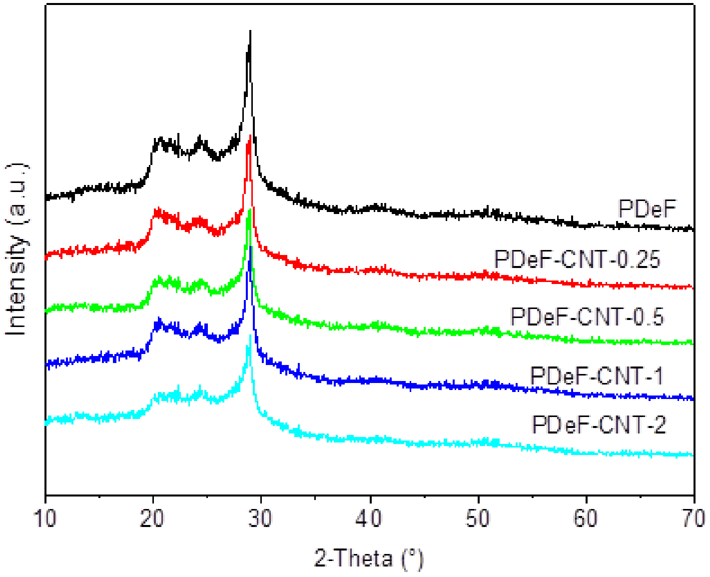

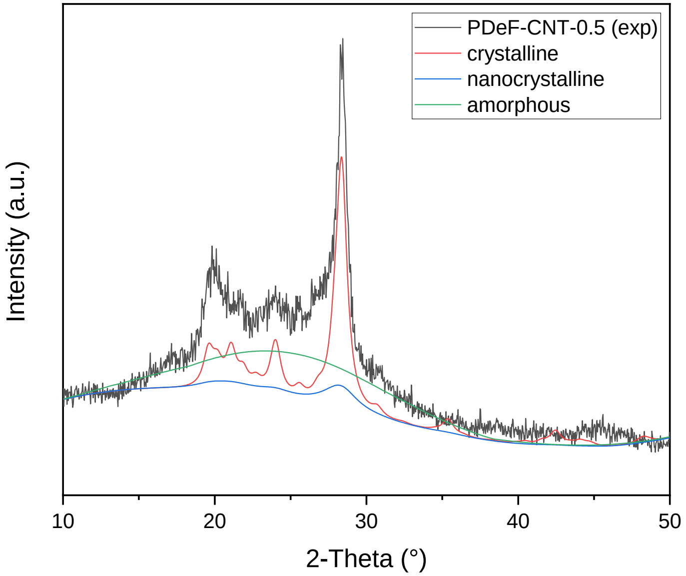

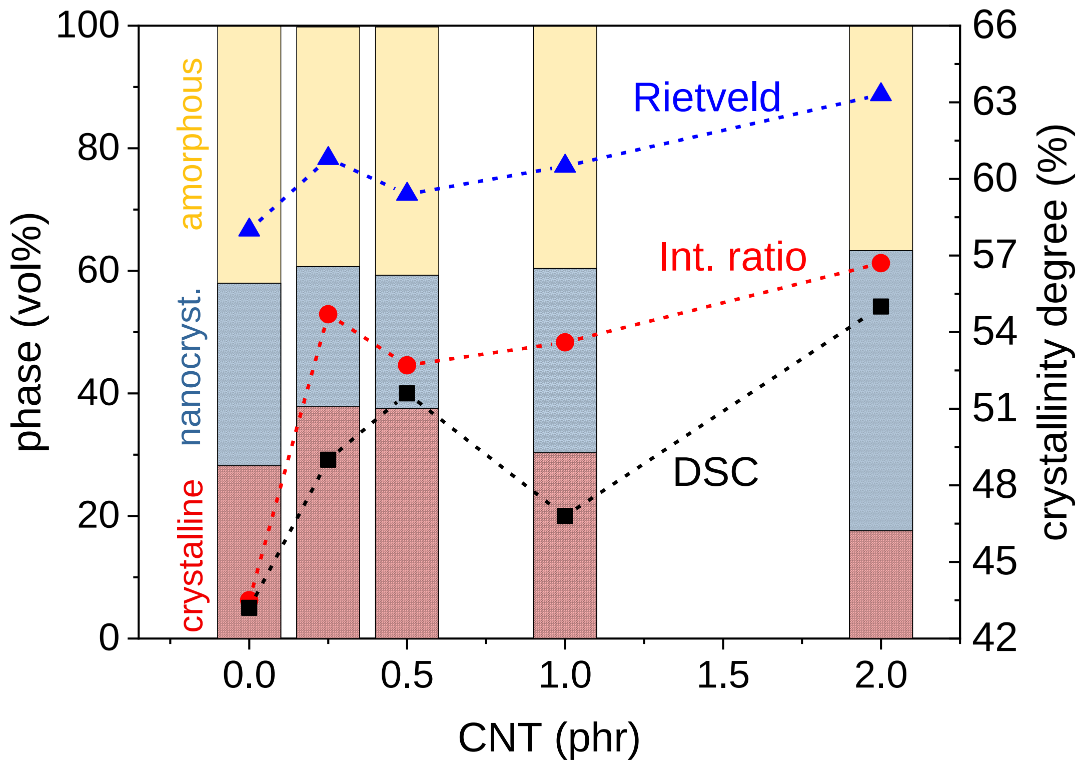

- **semicrystalline**: sharp Bragg reflections + amorphous halo
- similar to XRD pattern of aromatic–aliphatic polyesters with long methylene chains → **triclinic β-form** assumed
- modeling of the **crystalline, nano(para)crystalline, and amorphous** fractions (Maud Rietveld software) → semi-quantitative evaluation of the crystallinity degree

- increase in **macrocrystalline** fraction at the expense of the nanocrystalline one until 0.5 phr of CNT, opposite trend for higher concentrations
- **Int. ratio (fitting) underestimates X_c** and gives values similar to those measured by DSC

*G. Fredi et al., Polymers **2020**, 12(11), 2459*

Tensile tests

Increase in crystallinity

+ refinement in microstructure

→ strengthening-toughening effect

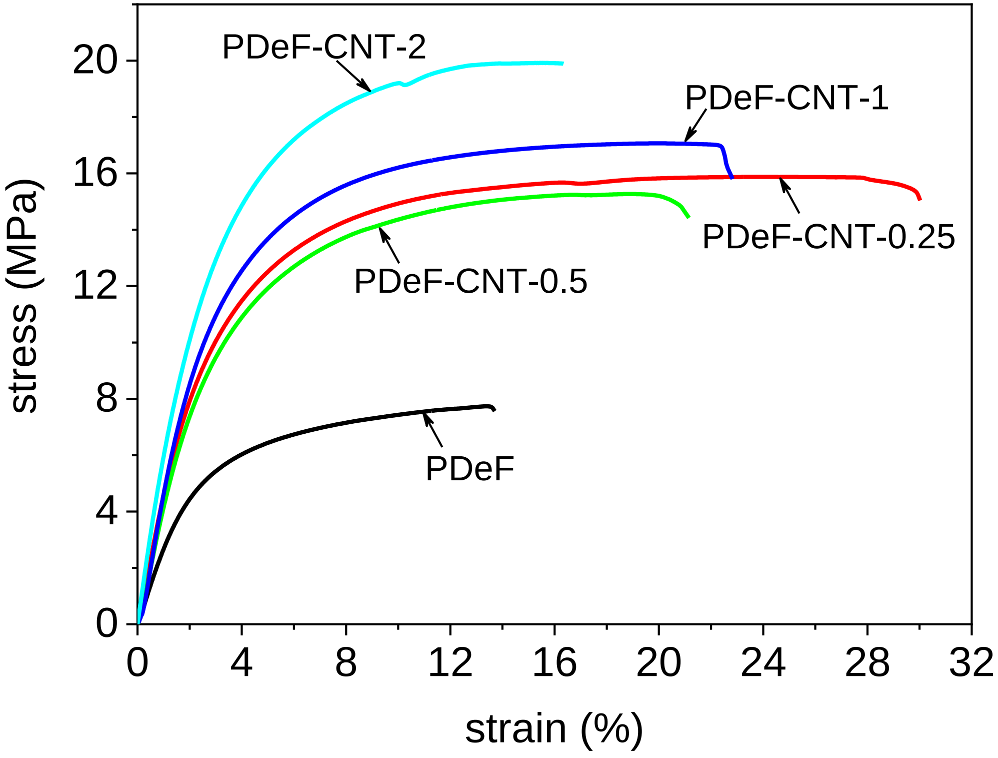

Instron 5969; gauge length 50 mm; 10 mm/min.

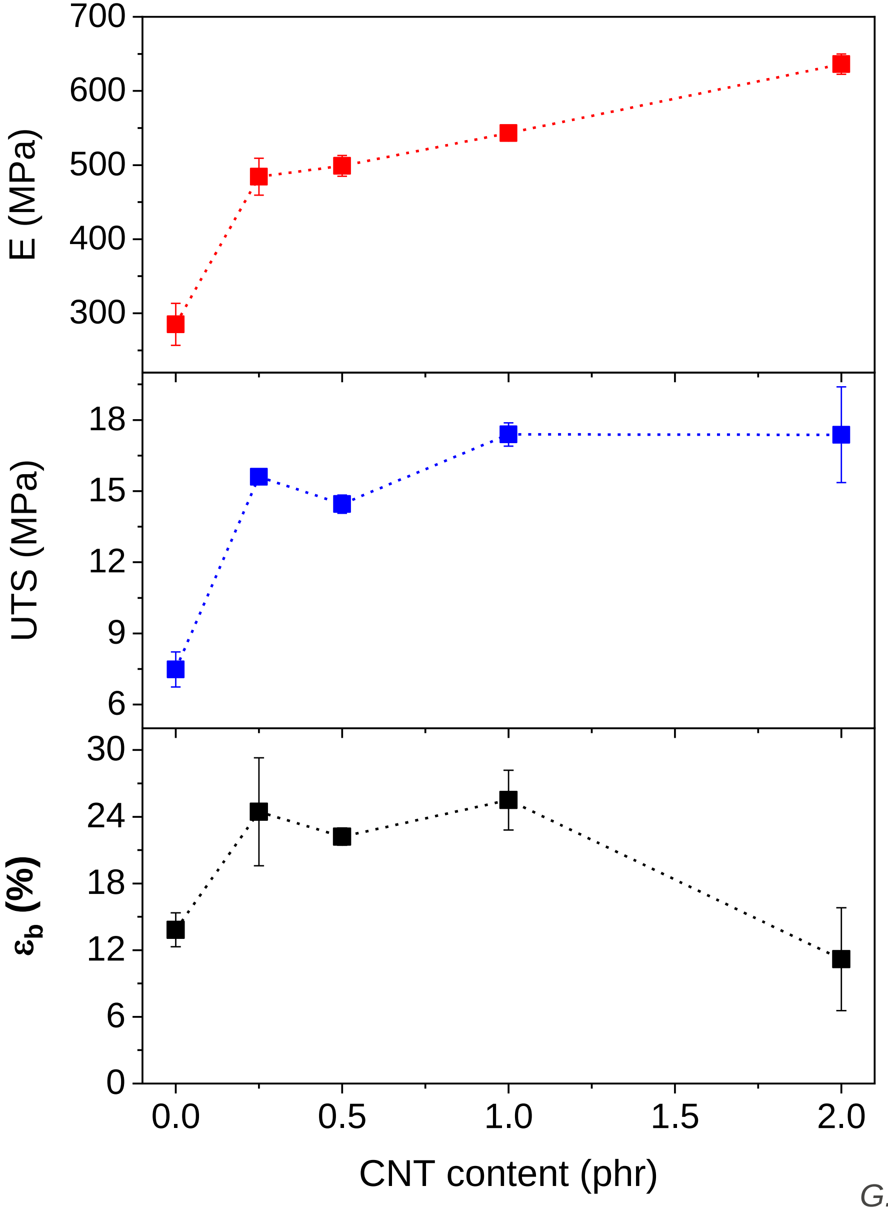

- **increase in elastic modulus**

+70% with 0.25 phr CNT
+123% with 2 phr CNT

- **increase in tensile strength**

+108% with 0.25 phr CNT
+131% with 2 phr CNT

- **increase in strain at break**

+180% with 0.25 phr CNT

*G. Fredi et al., Polymers **2020**, 12(11), 2459*

Dynamic mechanical thermal analysis (DMTA)

TA DMA Q800; tensile mode; 0.05 % strain

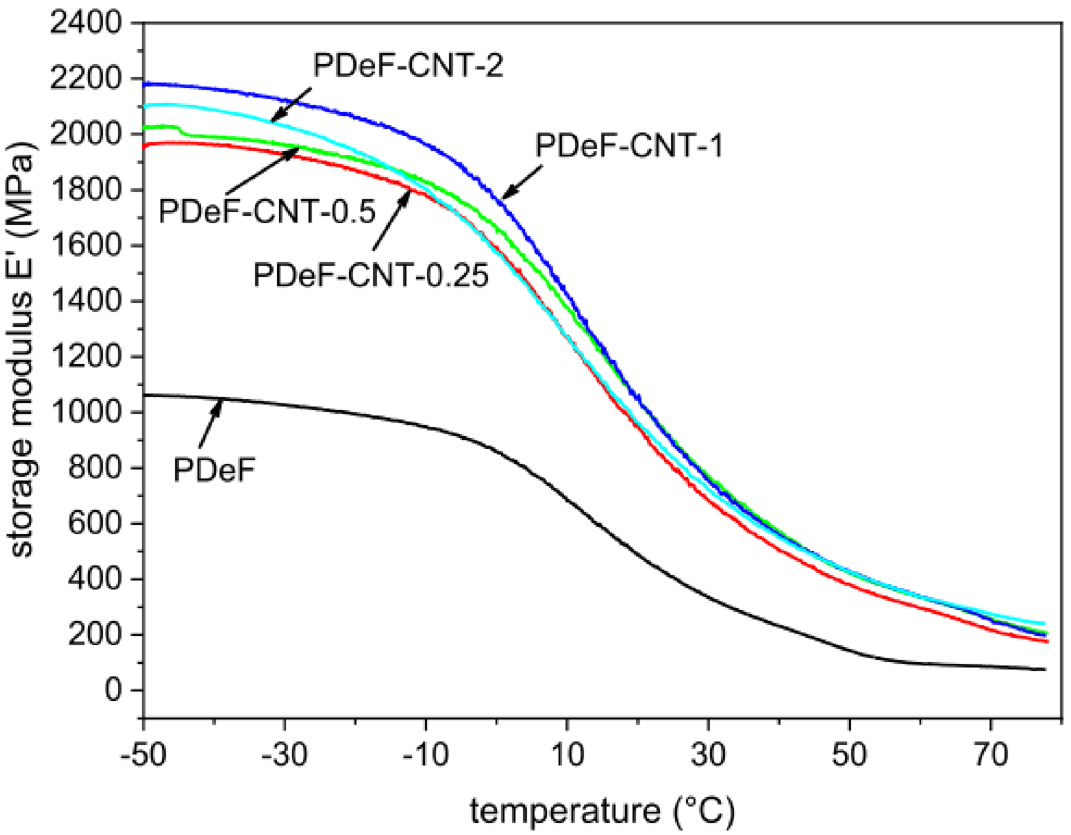

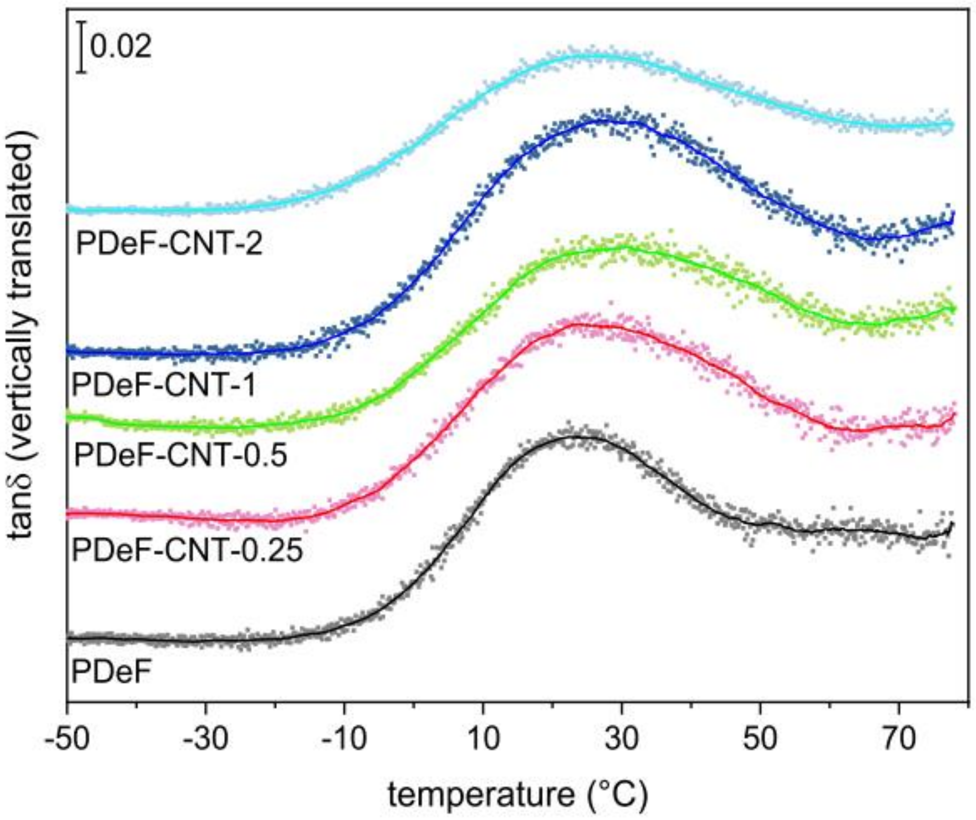

- E' increases for CNT nanocomposites, up to 2023 MPa at -50 °C for PDeF-CNT-2 (+93% vs neat PDeF).
- T_g shifted to higher values with CNT addition, indicating CNTs restricted mobility of PDeF amorphous regions
- Height of tanδ peak was not significantly affected by CNT content

→ Increase in strain at break with CNTs attributed to reduced crystallite size rather than increased molecular mobility.

*G. Fredi et al., Polymers **2020**, 12(11), 2459*

2. PLA/PDoF+ rGO

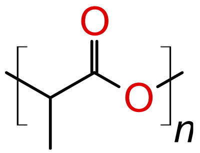

polylactide

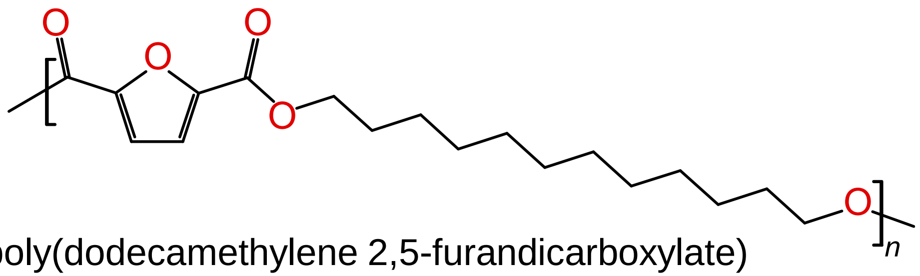

poly(dodecamethylene 2,5-furandicarboxylate)

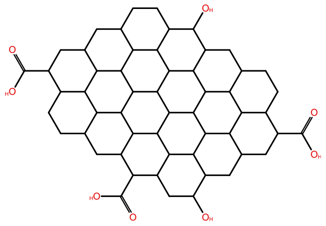

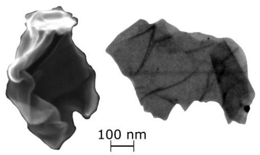

reduced graphene oxide

PLA/PDoF/rGO nanocomposites

Polylactide (PLA)

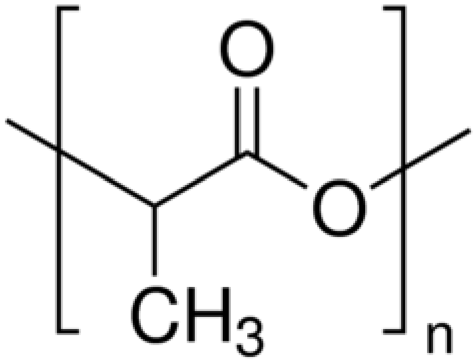

- widely used **biobased** and **biodegradable** biopolymer
- properties depend on the relative fraction of L- and D-lactide
- Commercial PLA: mostly **PLLA** with 2-4 % of D-lactide

- high **elastic modulus** (2-3 GPa)
- good mechanical **strength** (40-60 MPa)
- good **processability**
- high optical **transparency**

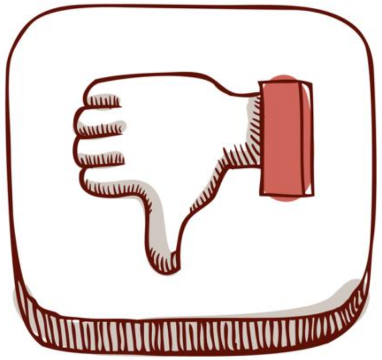

- poor **strain at break and toughness**
- high **moisture** sensitivity
- low **gas barrier** properties
- poor UV-shielding properties

PLA/PDoF/rGO nanocomposites

Prepare and characterize nanocomposite films

- **PLA** + **PDoF (10 wt%)** blend
- **rGO (0.25 to 2 phr)** as a **multifunctional** nanofiller

- Blend compatibility
- Crystallization kinetics
- Mechanical properties
- Antistatic properties
- Gas barrier properties

Packaging applications

Polylactide (**PLA**)

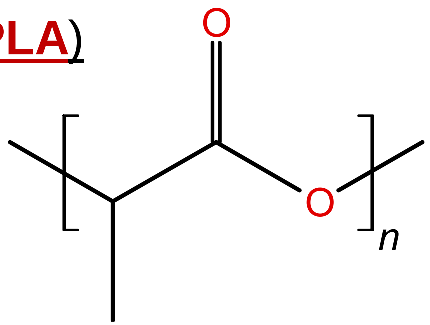

Poly(dodecamethylene furanoate) (**PDoF**)

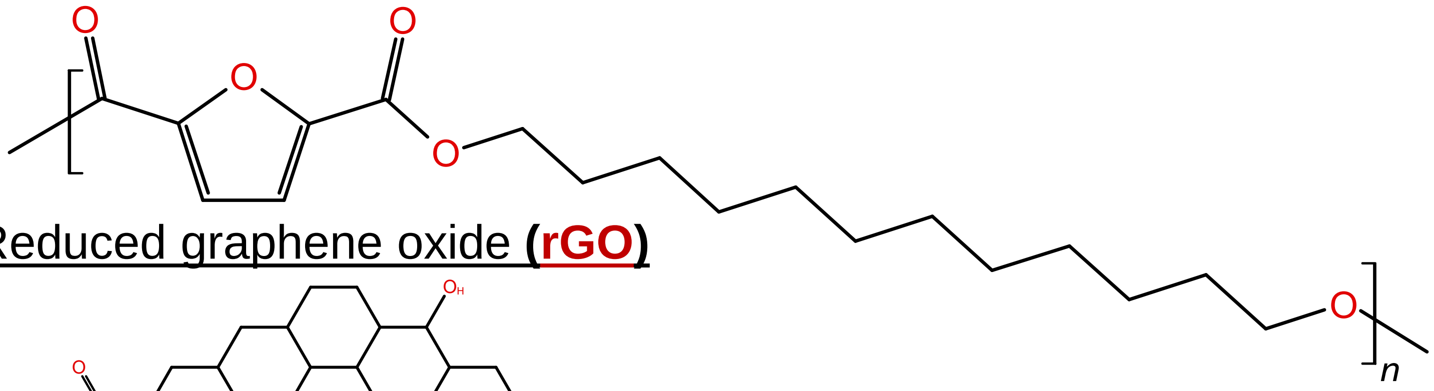

Reduced graphene oxide (**rGO**)

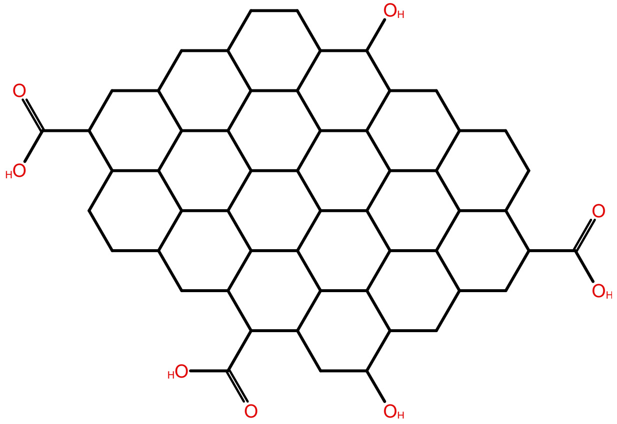

G. Fredi et al., Molecules, vol. 26, p. 2398, 2021

Microstructure

FE-SEM Zeiss Supra 60; cryofracture surfaces

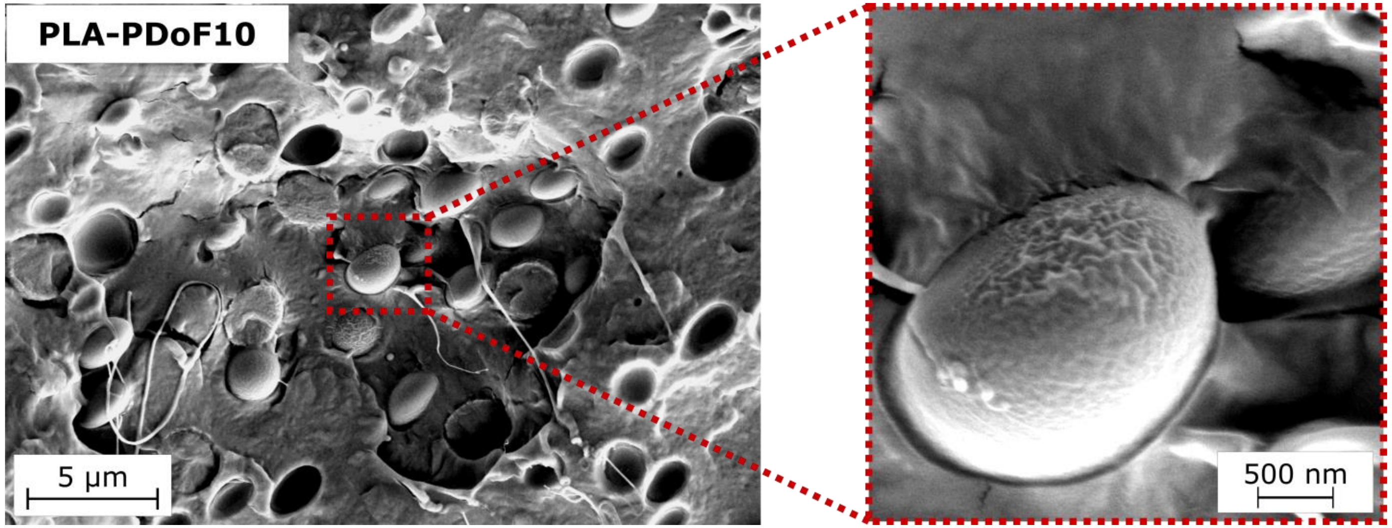

PLA-PDoF10

- immiscible blend
- PDoF spheroidal domains (**2.6 ± 0.4 µm**)

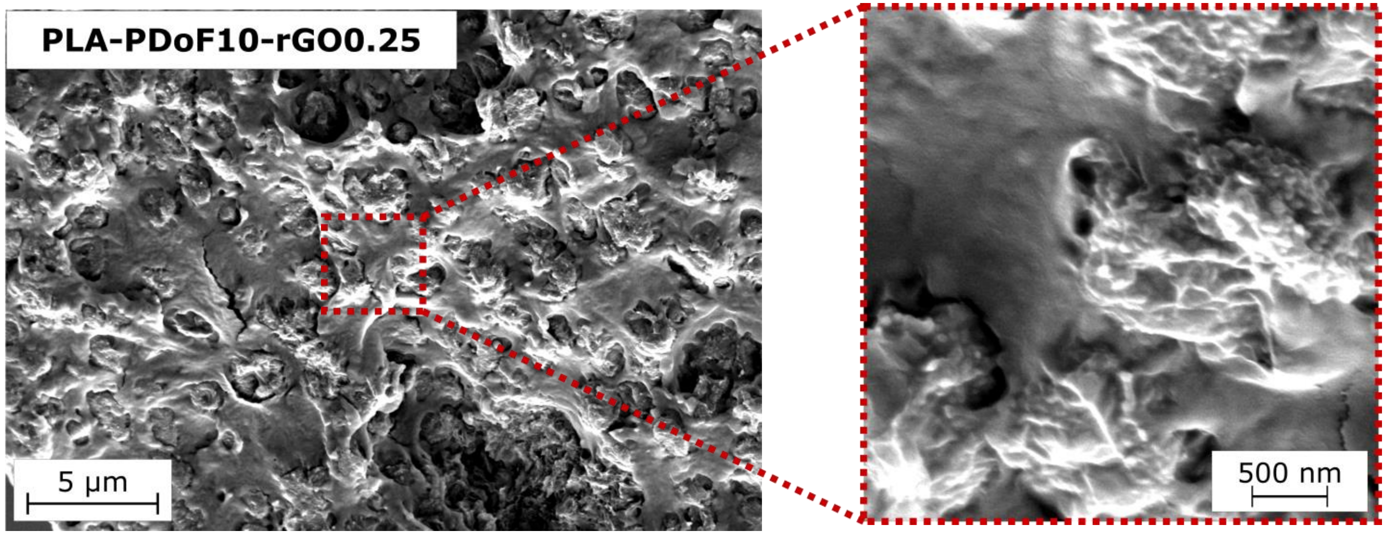

PLA-PDoF10-rGO0.25

- rGO preferentially distributed in the PDoF domains
- PDoF domains are rougher and smaller (**1.6 ± 0.3 µm**)
- ↑ interfacial interaction

G. Fredi et al., Molecules, vol. 26, p. 2398, 2021

Microstructure

FE-SEM Zeiss Supra 60; cryofracture surfaces

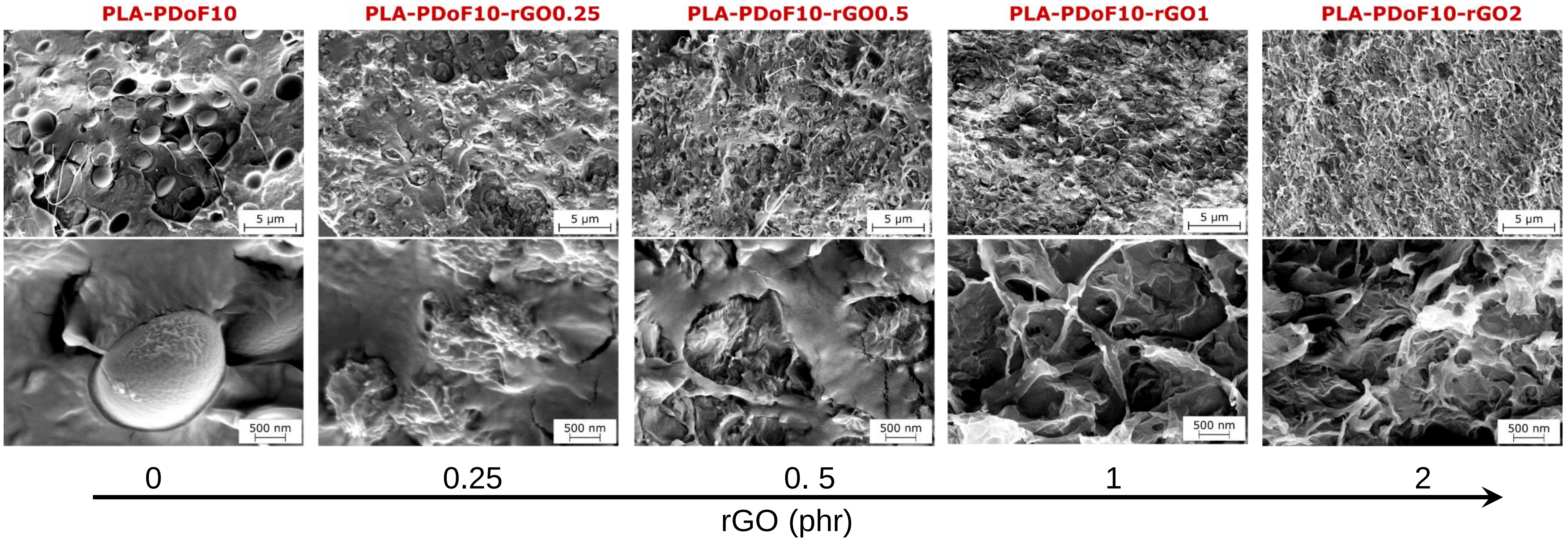

- morphological changes in PDoF domains and in the fracture surface with an increase in the rGO concentration
- rGO agglomeration at high concentrations

G. Fredi et al., Molecules, vol. 26, p. 2398, 2021

Sample preparation

1) GO chemical reduction to rGO

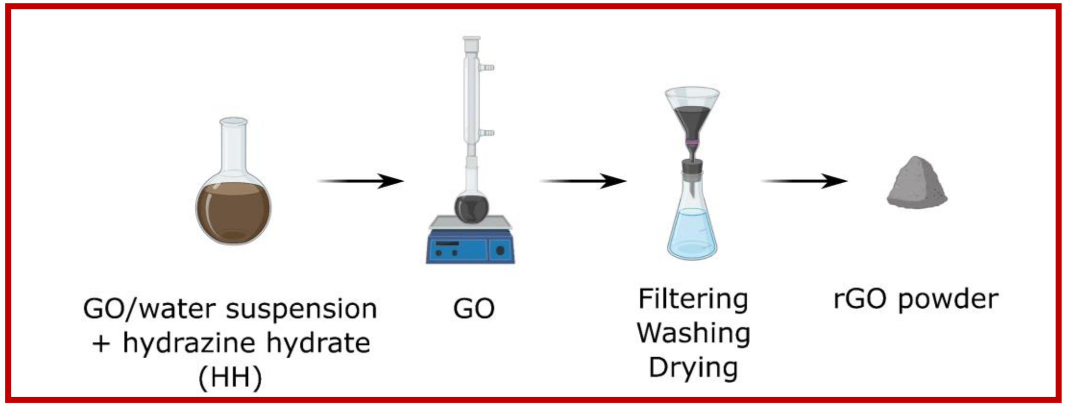

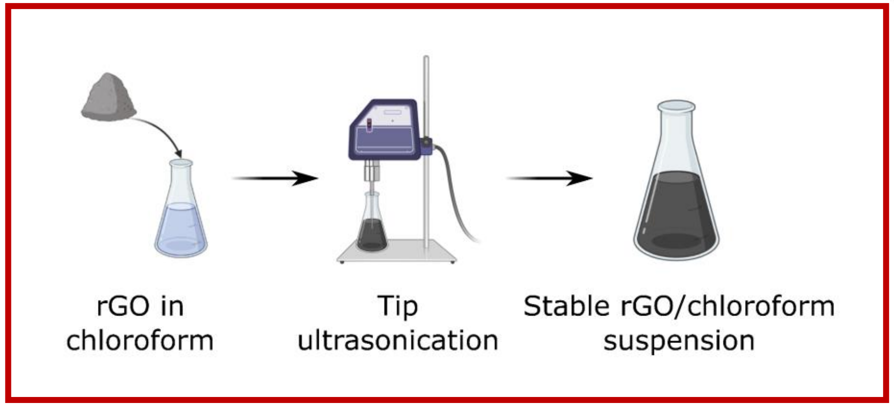

3) Solvent casting

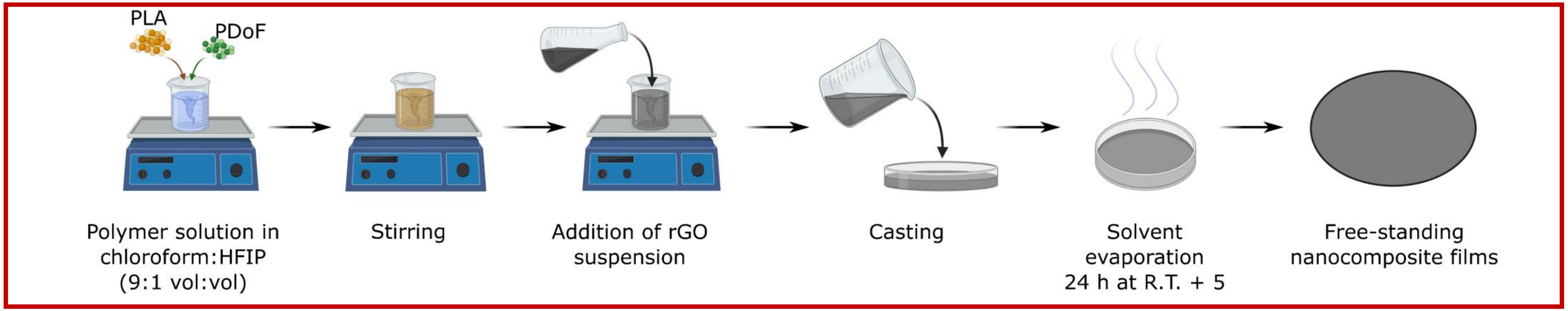

Sample	PLA (wt%)	PDoF (wt%)	rGO (phr)
PLA	100	0	0
PLA-rGO0.25	100	0	0.25
PLA-rGO2	100	0	2
PLA-PDoF10	90	10	0

Sample	PLA (wt%)	PDoF (wt%)	rGO (phr)
PLA-PDoF10-rGO0.25	90	10	0.25
PLA-PDoF10-rGO0.5	90	10	0.5
PLA-PDoF10-rGO1	90	10	1
PLA-PDoF10-rGO2	90	10	2

G. Fredi et al., Molecules, vol. 26, p. 2398, 2021.

Differential scanning calorimetry (DSC)

Mettler Toledo DSC 30 calorimeter; 10 ° C/min; heating/cooling/heating; nitrogen flow 100 ml/min

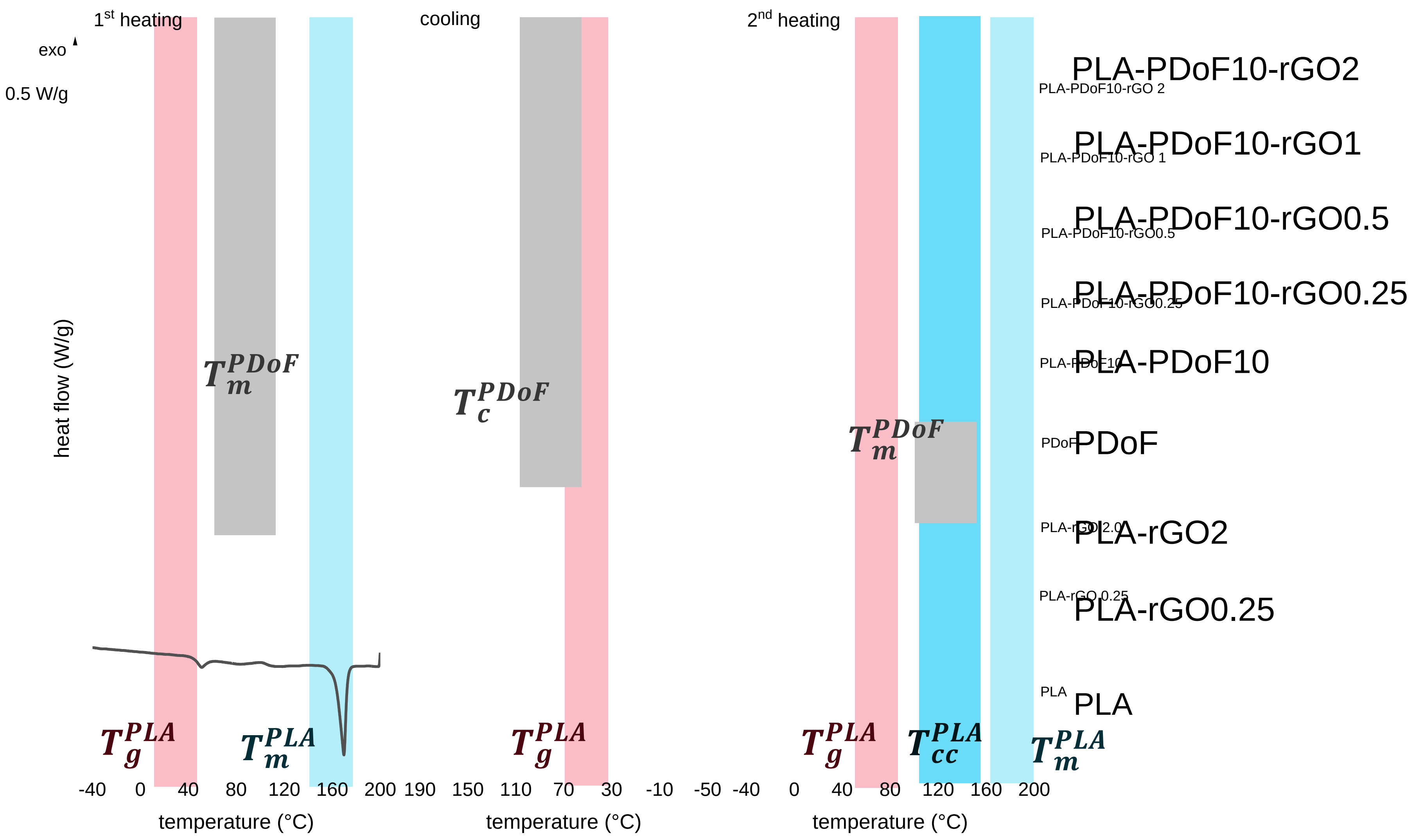

G. Fredi et al., Molecules, vol. 26, p. 2398, 2021

Differential scanning calorimetry (DSC)

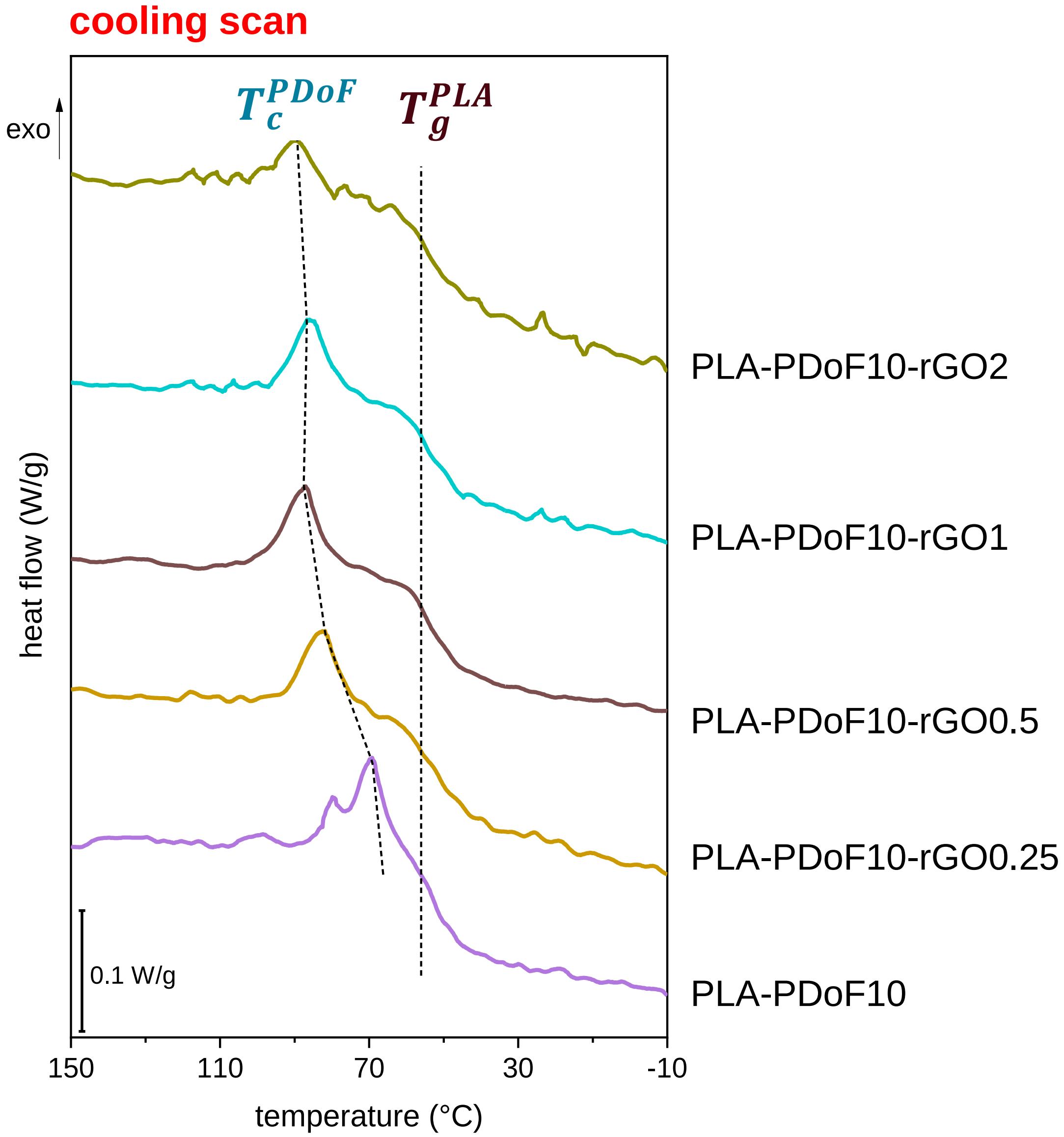

T_g^{PLA} stable ⇒ immiscibility

T_c^{PDoF} increases by increasing rGO concentration:
⇒ rGO promotes PDoF crystallization

Sample	**rGO (phr)**	T_c^{PDoF} **(°C)**
PDoF	0	68.5
PLA-PDoF10	0	69.3
PLA-PDoF10-rGO0.25	0.25	82.0
PLA-PDoF10-rGO0.5	0.5	86.3
PLA-PDoF10-rGO1	1	87.7
PLA-PDoF10-rGO2	2	89.7

G. Fredi et al., Molecules, vol. 26, p. 2398, 2021

Differential scanning calorimetry (DSC)

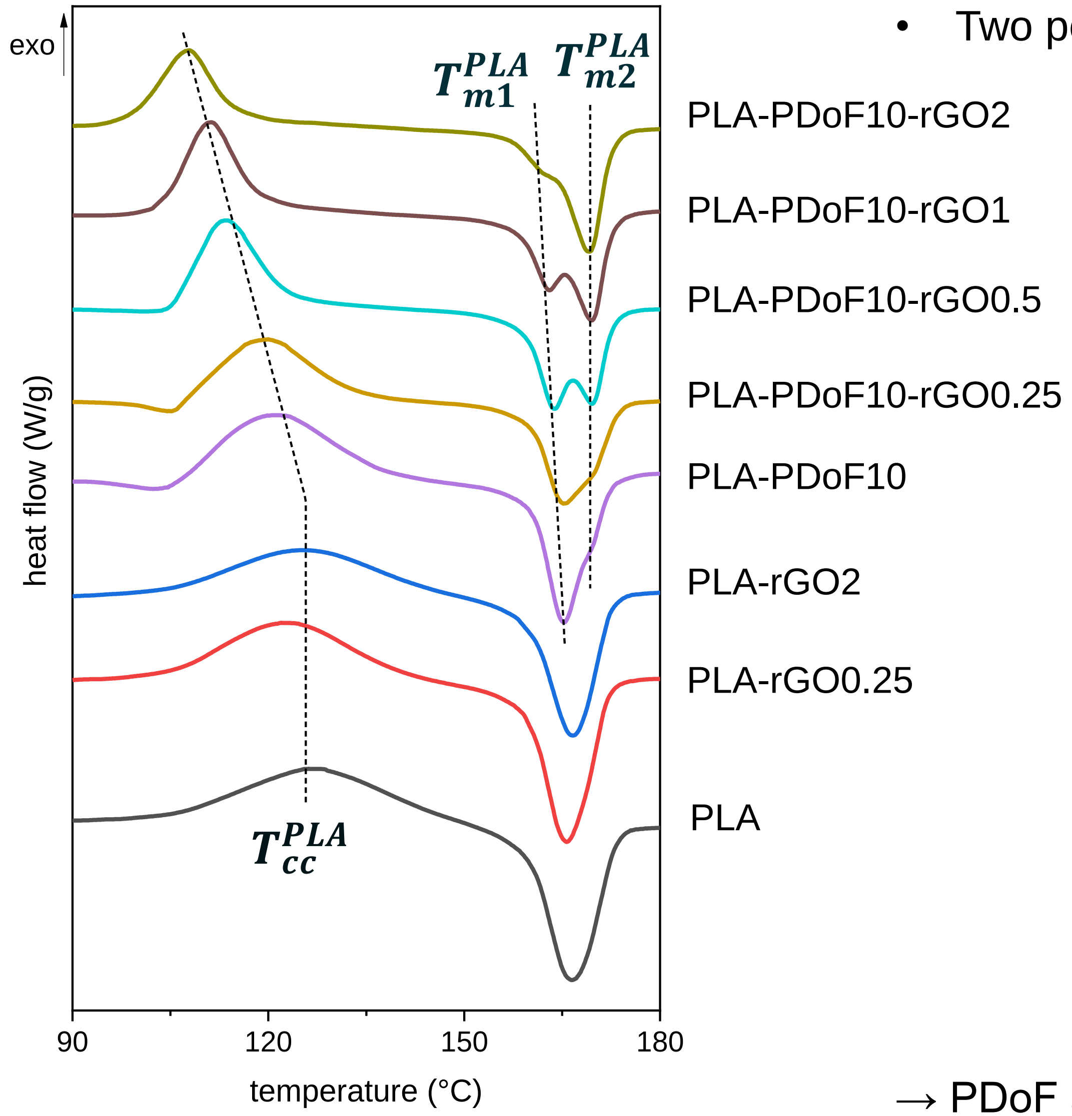

- T_{cc}^{PLA} decreases with rGO, especially when PDoF is present
- Two peaks in PLA melting

Sample	rGO (phr)	2nd HS X_c^{PLA} (%)	1st HS X_c^{PLA} (%)
PLA	0	2.3	41.3
PLA-rGO0.25	0.25	5.2	38.6
PLA-rGO2	2	5.4	36.0
PLA-PDoF10	0	1.3	35.9
PLA-PDoF10-rGO0.25	0.25	4.8	32.0
PLA-PDoF10-rGO0.5	0.5	6.6	34.9
PLA-PDoF10-rGO1	1	8.5	33.7
PLA-PDoF10-rGO2	2	6.3	35.0

$$X_c^{PLA} = \frac{\Delta H_m^{PLA} - \Delta H_{cc}^{PLA}}{w \cdot \Delta H_0^{PLA}} \cdot 100$$

→ PDoF and rGO **synergistically** improve PLA crystallization

G. Fredi et al., Molecules, vol. 26, p. 2398, 2021

Mechanical properties

Instron 5969; gauge length 50 mm; 10 mm/min.

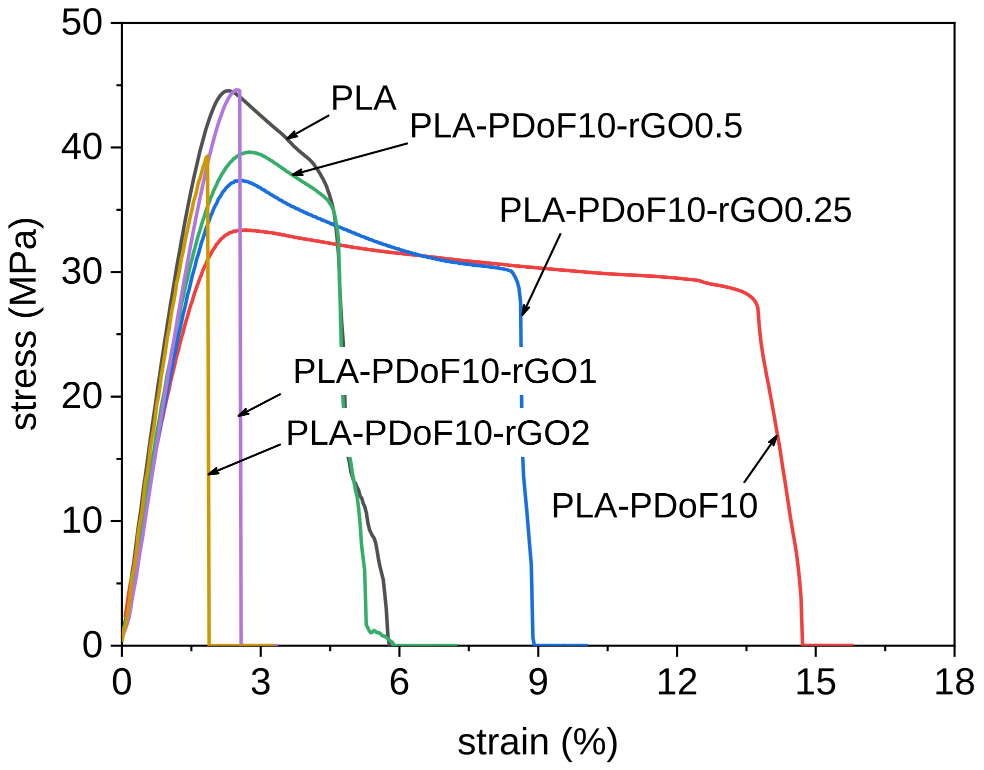

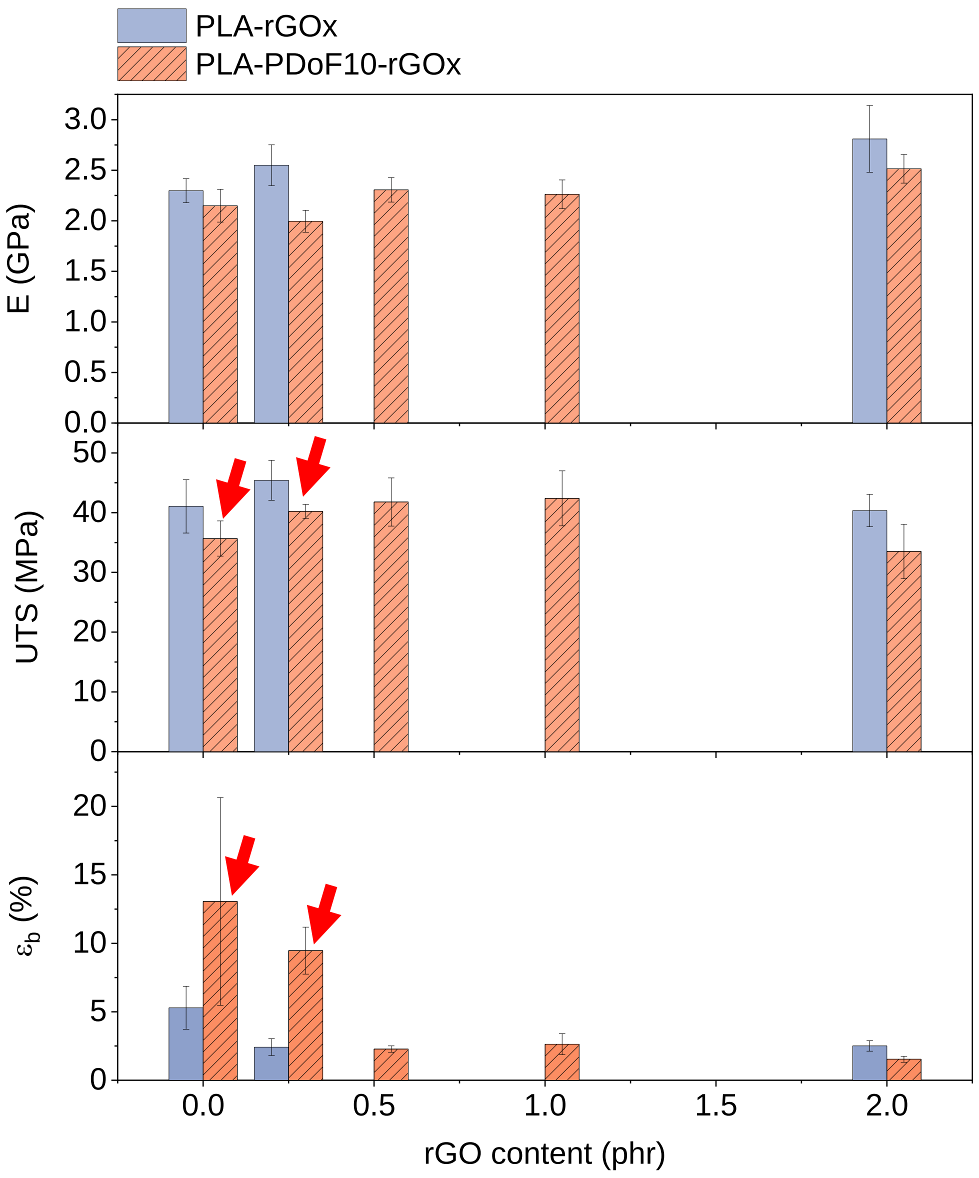

- PDoF at 10 wt% enhances PLA ductility
- the contribution of rGO is rather modest
- further improvements may be obtained with a lower rGO content (e.g., 0.1 phr)

G. Fredi et al., Molecules, vol. 26, p. 2398, 2021

Gas barrier properties

Gas phase permeation; R.T.; Quadrupole Mass Spectrometer (QMS, Balzers QMG 420);
Roilo et al., Surf. Coat. Technol. 2018, 343, 131-137.

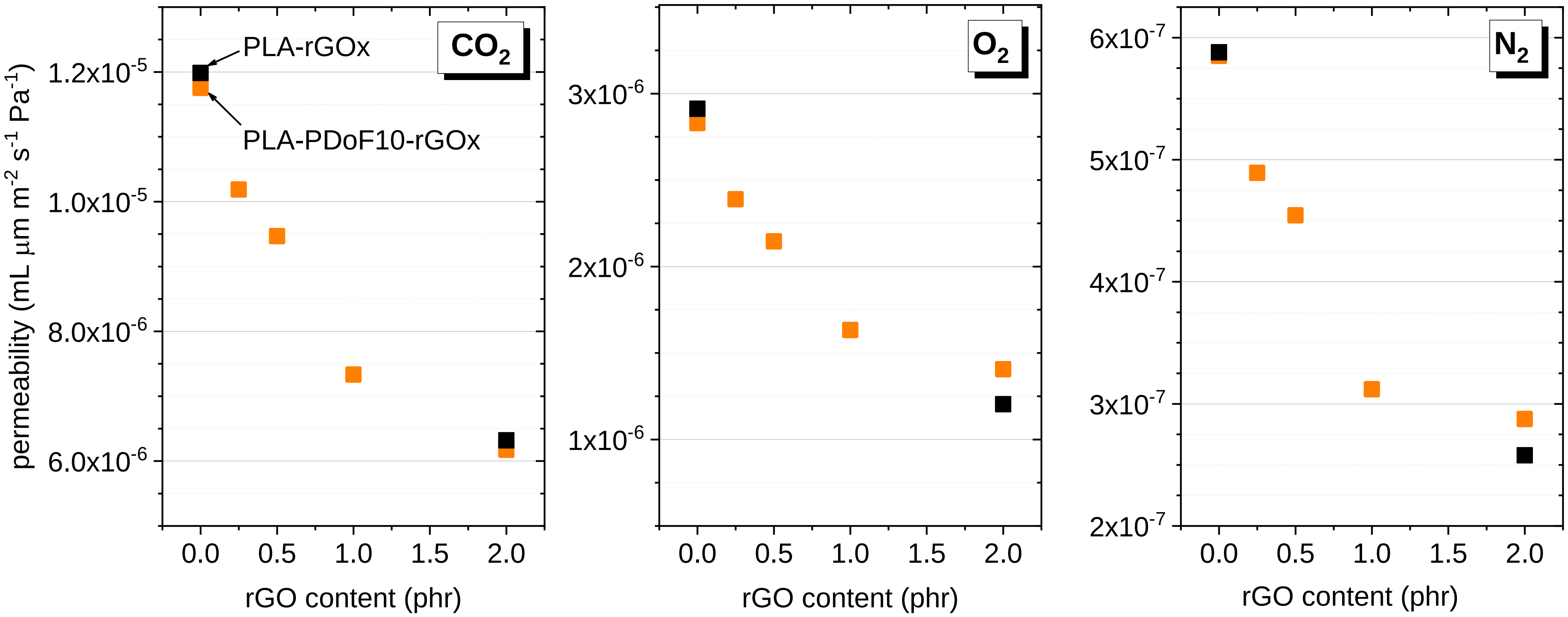

- Both **permeability** and **diffusivity** decrease by increasing rGO fraction
- Data for all gases are comparable

⇒ improvement of the gas barrier properties due to:

- **reduced gas mobility** rather than to a decreased gas solubility
- **longer diffusion paths** for gas molecules

G. Fredi et al., Molecules, vol. 26, p. 2398, 2021

Gas barrier properties

Gas phase permeation; R.T.; Quadrupole Mass Spectrometer (QMS, Balzers QMG 420);
Roilo et al., Surf. Coat. Technol. 2018, 343, 131-137.

Data of PLA-PDoF10-rGOx

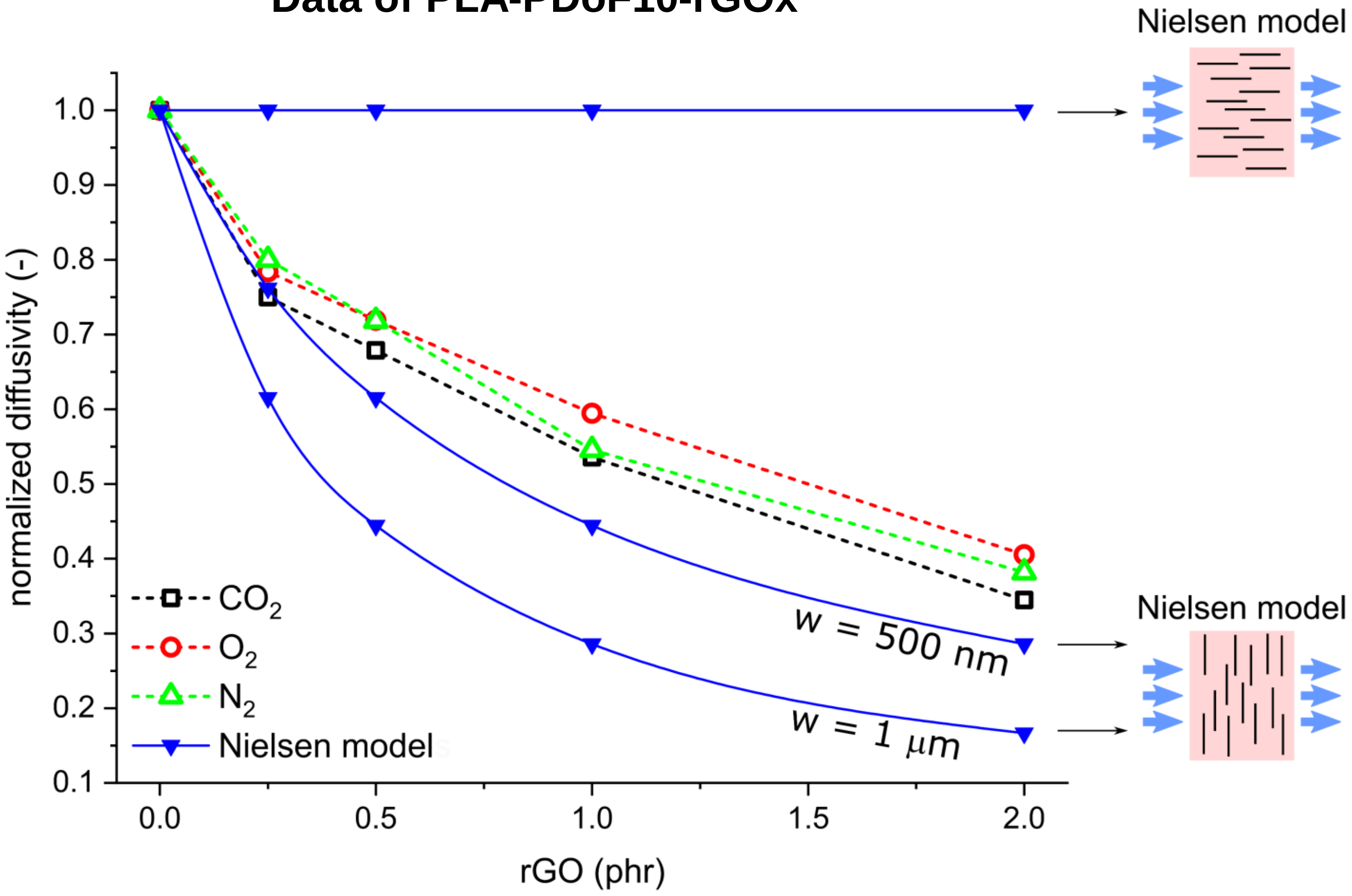

Nielsen model for the diffusivity

$$\frac{D}{D_0} = \frac{1}{\tau}$$

D = nanocomposite diffusivity
D_0 = matrix diffusivity

$$\tau = 1 + \frac{1}{2}\,\alpha\,\varphi$$

φ = nanofiller volume fraction
α = nanofiller aspect ratio = **w / th**

rGO after sonication

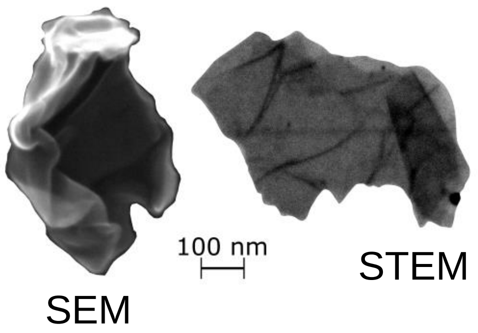

G. Fredi et al., Molecules, vol. 26, p. 2398, 2021

Conclusions: 2 main take-home messages

PDeF/CNT

microstructural homogenization provided by CNTs increases toughness

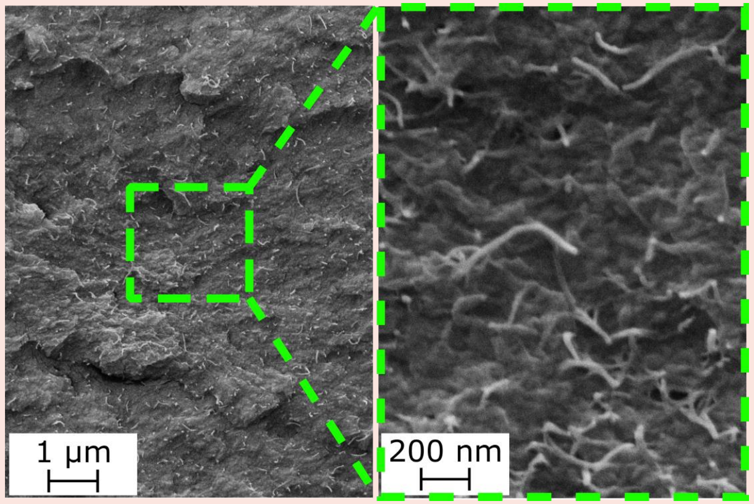

[1] G. Fredi et al., *Polymers*, ***2020, 12, 2459.***

PLA/PDoF/rGO

rGO is a multifunctional nanofiller

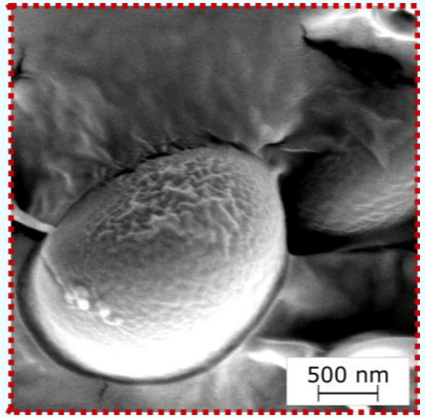

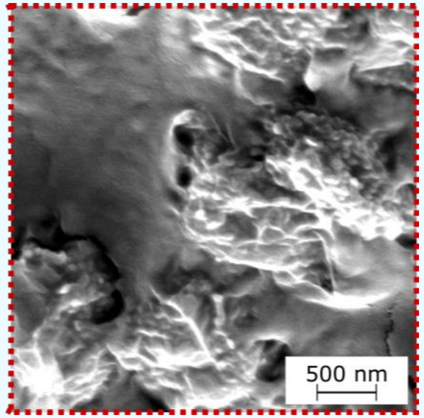

[2] G. Fredi et al., *Molecules*, ***2021, 26, 2398***
[3] G. Fredi et al., *Materials*, ***2022, 15, 1316***

Giulia Fredi
giulia.fredi@unitn.it